AGU PUBLICATIONS

Geophysical Research Letters

RESEARCH LETTER
10.1002/2016GL069157

Special Section:
First results from NASA's Magnetospheric Multiscale (MMS) Mission

MMS Multipoint electric field observations of small-scale magnetic holes

Katherine A. Goodrich[1], Robert E. Ergun[1], Frederick D. Wilder[1], James Burch[2], Roy Torbert[3], Yuri Khotyaintsev[4], Per-Arne Lindqvist[5], Christopher Russell[6], Robert Strangeway[6], Werner Magnes[7], Daniel Gershman[8], Barbara Giles[8], Rumi Nakamura[7], Julia Stawarz[1], Justin Holmes[1], Andrew Sturner[1], and David M. Malaspina[1]

[1]Department of Astrophysical and Planetary Sciences, University of Colorado Boulder, Boulder, Colorado, USA, [2]Southwest Research Institute, San Antonio, Texas, USA, [3]Department of Physics, University of New Hampshire, Durham, New Hampshire, USA, [4]Swedish Institute of Space Physics, Uppsala, Sweden, [5]Royal Institute of Technology, Stockholm, Sweden, [6]Department of Earth, Planetary and Space Science, University of California, Los Angeles, California, USA, [7]Space Research Institute, Austrian Academy of Sciences, Graz, Austria, [8]NASA Goddard Space Flight Center, Greenbelt, Maryland, USA

Key Points:
- MMS shows multipoint electric field observations of a small-scale magnetic hole
- Electric field observations suggest small-scale magnetic holes are supported by perpendicular electron currents
- MMS observations suggest that small-scale magnetic holes can cascade to smaller spatial scales

Correspondence to:
K. A. Goodrich,
katherine.goodrich@lasp.colorado.edu

Citation:
Goodrich, K. A., et al. (2016), MMS Multipoint electric field observations of small-scale magnetic holes, *Geophys. Res. Lett.*, *43*, 5953–5959, doi:10.1002/2016GL069157.

Received 14 APR 2016
Accepted 16 MAY 2016
Accepted article online 23 MAY 2016
Published online 20 JUN 2016

Abstract Small-scale magnetic holes (MHs), local depletions in magnetic field strength, have been observed multiple times in the Earth's magnetosphere in the bursty bulk flow (BBF) braking region. This particular subset of MHs has observed scale sizes perpendicular to the background magnetic field (B) less than the ambient ion Larmor radius (ρ_i). Previous observations by Time History of Events and Macroscale Interactions during Substorms (THEMIS) indicate that this subset of MHs can be supported by a current driven by the $E \times B$ drift of electrons. Ions do not participate in the $E \times B$ drift due to the small-scale size of the electric field. While in the BBF braking region, during its commissioning phase, the Magnetospheric Multiscale (MMS) spacecraft observed a small-scale MH. The electric field observations taken during this event suggest the presence of electron currents perpendicular to the magnetic field. These observations also suggest that these currents can evolve to smaller spatial scales.

1. Introduction

MHs are observed depressions in magnetic field strength $|B|$. They are seen in many space plasmas such as the solar wind [*Russell et al.*, 2008; *Winterhalter et al.*, 1995], the heliosheath *Burlaga et al.* [2007], the terrestrial magnetosheath [*Soucek et al.*, 2008; *Johnson and Cheng*, 1997], and the near-Earth plasma sheet [*Ge et al.*, 2011; *Balikhin et al.*, 2012; *Sun et al.*, 2012; *Sundberg et al.*, 2015; *Goodrich et al.*, 2016]. MHs significantly larger than the ion Larmor radius (ρ_i) can be explained by the mirror-mode instability [*Southwood and Kivelson*, 1993]. Conversely, small-scale MHs ($< \rho_i$) cannot be explained by MHD-scale mechanisms like the mirror-mode instability.

Small-scale MHs have been mostly observed in the bursty bulk flow (BBF) braking region [*Ge et al.*, 2011; *Sundberg et al.*, 2015]. The BBF braking region is located in the near-Earth plasma sheet (6–12 R_E). It has been well documented as a region of strong plasma turbulence [*Cattell and Mozer*, 1982; *Angelopoulos et al.*, 1999; *Borovsky et al.*, 1997; *Weygand et al.*, 2005; *Vörös et al.*, 2006; *Ergun et al.*, 2015; *Stawarz et al.*, 2015]) due to strong Earthward flows originating from magnetic reconnection in the magnetotail [*Baumjohann et al.*, 1989; *Ohtani et al.*, 2004; *Runov et al.*, 2009, 2011; *Sitnov et al.*, 2009; *Fu et al.*, 2013].

Some of these small-scale MHs have observed hole diameters in the order of tens of ρ_e (hundreds of kilometers) and show a magnetic field decrease of ~10–20% from its initial $|B|$ value. This type of small-scale MHs have been observed by Cluster [*Sundberg et al.*, 2015] and Time History of Events and Macroscale Interactions during Substorms (THEMIS) [*Ge et al.*, 2011] and now by MMS [*Gershman et al.*, 2016]. *Gershman et al.* [2016] in particular found strong electron currents, measured by Fast Plasma Investigation [*Pollock et al.*, 2016], associated with the small-scale MH. These structures appear stable and even in pressure balance. Such structures were also found to form in kinetic plasma turbulence simulations [*Haynes et al.*, 2015]. In these simulations, this group of small-scale MHs appears to be stable over many electron gyroperiods.

Small-scale MHs with larger hole diameters (tens of ρ_e to $> \rho_i$, or order of 100 to 1000 km) have also been observed by *Sun et al.* [2012], *Tenerani et al.* [2012, 2013], and *Goodrich et al.* [2016]. These small-scale MHs show observed $|B|$ deviations ~50–80% from initial $|B|$ value. Though they have a larger observed diameter size, they also are characterized by electric field signatures that were indicative of a very thin current layer ($< \rho_i$, ~10–100 km), which were shown to be largely electron populated. These currents were perpendicular to the background magnetic field direction and sufficient to induce the observed change in $|B|$.

A relationship between these two types has not yet been investigated. It is not known whether they share the same physical processes. The cause or generation mechanism for both groups of small-scale MHs is currently unconfirmed, though several theories have been put forward. *Ji et al.* [2014] suggest that small-scale MHs are evidence of magnetosoliton waves. *Balikhin et al.* [2012] proposes that small-scale MHs are formed through remnants of the tearing instability in the deep tail.

The MMS mission [*Burch et al.*, 2016] now offers a unique perspective into these small-scale structures. On 2 June 2015, while in its commissioning phase, the MMS spacecraft observe both types of MHs in a single event. The MMS commissioning phase took place between March and September 2015. During this time the spacecraft travel in near-identical orbits with a maximum separation of approximately 260 km and orbit apogees positioned well into the BBF region. During the time of this event, all particle instruments were powered off. The entire FIELDS Instrument suite [*Torbert et al.*, 2016], however, was operational. The close proximity of the spacecraft allow multipoint electric (E) and magnetic (B) field measurements of a small-scale MH with a spatially smaller MH embedded inside it. The E field measurements associated with these MHs provide additional evidence of electron currents due to $E \times B$ drifting electrons. MMS also suggests that electron currents are present in both types of small-scale MHs, strongly implying that they are driven by the same processes.

2. Data and Observations

The data used for this analysis consist of magnetic field data from the flux gate magnetometers (FGM) [*Russell et al.*, 2014] and the combined electric field measurements from the spin plane double probes [*Lindqvist et al.*, 2016] and axial double probes [*Ergun et al.*, 2016]. The measurements are from a single small-scale MH event observed at ~01:47 UTC on 2 June 2015. The maximum separation, between MMS4 and MMS1, was ~260 km. The event was located in the near-Earth plasma sheet at ~−11 X_{GSE}, ~4 Y_{GSE}, and 0.8 Z_{GSE}. The longest duration of the event is seen on MMS4 for approximately 5 s. Electric field measurements were successfully obtained from MMS1, MMS3, and MMS4. The electric field data from MMS2 are not used due to nonoptimal bias settings, which caused oversaturation on the E field probes.

An overview of the MH event is shown in Figure 1. Figure 1a (first panel) shows the total magnetic field strength from all four spacecraft. Figures 1a (second panel) to 1a (fourth panel) show the associated electric field measurements from MMS1, MMS3, and MMS4 in descending order in the rotated coordinate system of the MH. *Mag* (red) is a component along the median magnetic field direction over the time of the magnetic hole event. *Flow* (blue) is a component along the median flow direction ($E \times B$ velocity used for rotation), and the *perp* component (green) completes the system. The four vertical lines outline the entering and exiting boundaries of the MH, identified by eye. This coordinate system is intended to view the field behavior as the magnetic hole directly passes the spacecraft in the flow direction. Figure 1b shows the relative formation of the spacecraft. The four spacecraft are in a close, linear formation (shown in Figure 1b) with MMS4 closest to Earth and each subsequent spacecraft positioned further tailward in ascending order. Figure 1c shows the apparent paths of the spacecraft across the MH event.

The MH is embedded in an area of strong magnetic field fluctuations. MMS4 sees the strongest change in $|B|$, with a decrease of ~75% of the initial $|B|$ value. The strength and size of the depression decreases from MMS4 to MMS1 in ascending order. The duration of the event extends between ~5 s on MMS4 and ~2 s on MMS2. MMS1 does not see a strong depression in $|B|$. The greatest E field activity occurs along the boundaries of the MH, indicated by the vertical lines aligned with the times in which MMS3 and MMS4 enters and exits the MH. Strong electric fields are observed on MMS3 and MMS4 along the boundaries of the event, whereas MMS1 observes increased activity along the center of the event.

3. Magnetic Hole Size and Motion

The positions of the spacecraft relative to the MH can be approximated using the direction of the electric fields. The E_{flow} component is the most significant on MMS4, indicating that it is closest to the center of the MH.

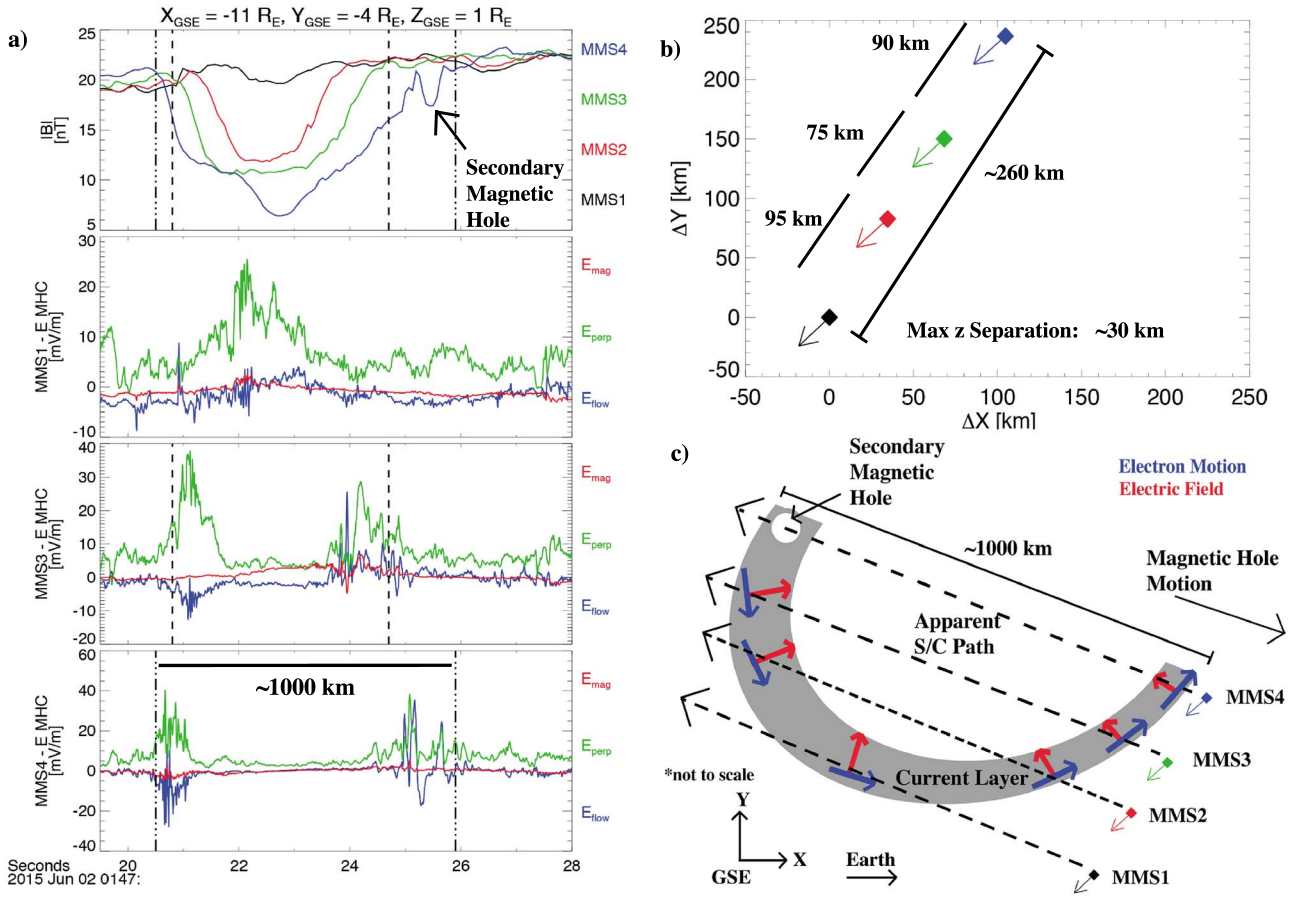

Figure 1. An overview plot of (a) the electric and magnetic fields observations from all four spacecraft (no electric field observations available on MMS2) in magnetic hole coordinates, a rotated coordinate system composed of the median magnetic field direction (mag, red), the median $E \times B$ velocity direction (flow, blue), and the remaining perpendicular direction (perp, green). (b) Spacecraft formation of all four MMS spacecraft in the *X*-*Y* plane (GSE coordinates), arrows indicating spacecraft motion, and (c) the estimated interaction between the magnetic hole and the spacecraft. The spacecraft are in a linear formation with a maximum separation of ~260 km in the *X*-*Y* plane and a maximum separation of 30 km along *Z*. The vertical lines indicate the beginning and end times of the magnetic hole on MMS3 and MMS4. Figure 1a (first panel) shows the total magnetic field strength from all four spacecraft. Figures 1a (second panel) to 1a (fourth panel) show the associated electric field measurements from MMS1, MMS3, and MMS4 in descending order in the rotated coordinate system of the MH.

The *E* field seen on MMS1 is most dominant in the perp direction, while E_{flow} shows a slight amplitude reversal. MMS1 observations are consistent with $E \times B$ drifting electrons reversing direction in the perp direction, implying that MMS1 passes through the edge of the current layer boundary of the MH.

The size and motion of the MH can be estimated using the velocity derived from geometric arguments and the known formation of the spacecraft. The observed decreases in $|B|$ are nested inside one another, implying that MMS2, MMS3, and MMS4 observe the structure simultaneously, while MMS1 encounters the very edge of the structure. These observations are consistent with an MH crossing the paths of the spacecraft obliquely. The spacecraft are positioned such that the motion of the MH must be primarily in the X_{GSE} direction with a moderate positive V_{YGSE} component if the MH travels earthward (and a negative V_{YGSE} component if directed antiearthward). The MH was seen first on MMS4, second on MMS3, and last on MMS1. The formation of the spacecraft implies that the MH traveling Earthward is the more likely scenario.

An approximate spatial scale and speed were estimated using the known position and formation of the spacecraft. Observations indicate that MMS1 passed through the outer edge of the current layer boundary. The nearest spacecraft to MMS1 is MMS2, which clearly passes through the interior of the MH (as it sees a stronger depression in $|B|$). We can therefore assume that the majority of the current layer is located inside the space that separates MMS1 and MMS2. The current layer at this time and location, therefore, must have a maximum width of 95 km (separation distance between MMS1 and MMS2). Using geometric arguments and

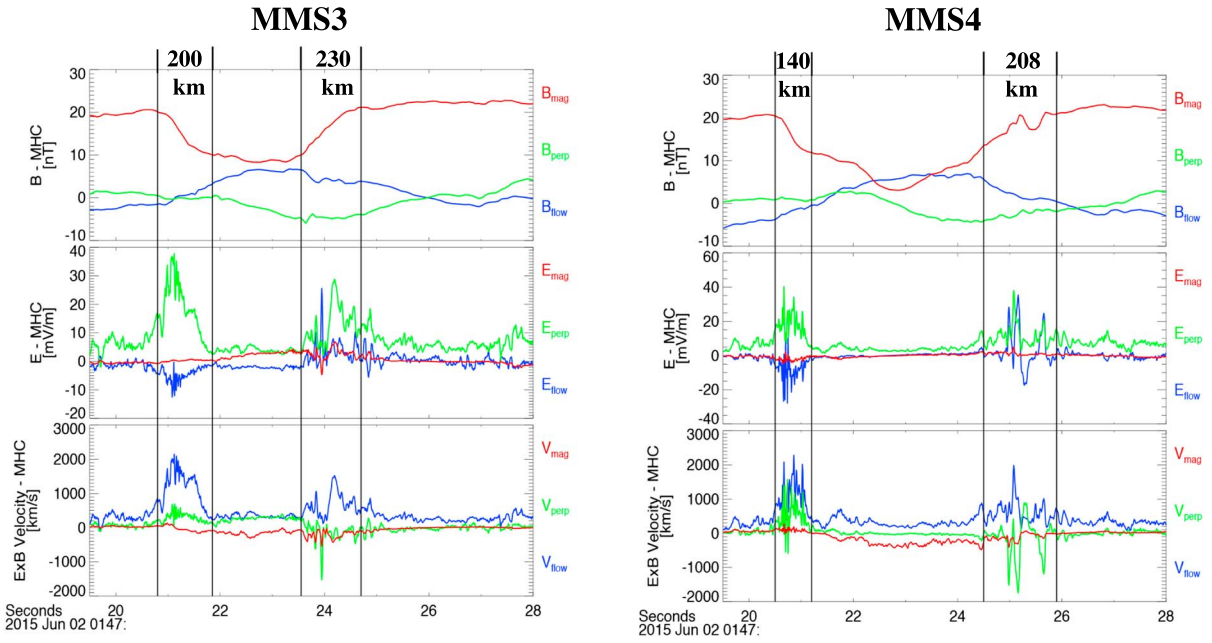

Figure 2. Magnetic field (top), electric (middle) field and $E \times B$ (V) velocity measurements for MMS3 (left) and MMS4 (right) in MH coordinates. There is little electric field activity along the mag direction and strong positive amplitude activity in the perp direction. The electric field along the flow direction shows negative amplitude activity along the entering boundary and positive amplitude activity along the exiting boundary.

considering the relative time in which MMS4 and MMS3 encounter the current layer, we estimate that the MH has an approximate diameter of 1000 km and travels across the spacecraft at ~160 km/s.

A median velocity was also derived using the 30 s interval directly prior to the MH event seen on MMS4. The velocity during the MH event was not used as it likely dominated activity from Hall currents and would not be indicative of the bulk motion of the structure. The median $E \times B$ velocity indicates the MH travels at −190 km/s and −60 km/s in the X_{GSE} and Y_{GSE} direction, respectively. There was a negligible motion observed in the Z_{GSE} direction (−2 km/s). This velocity indicates that the MH has a diameter of 1250 km, consistent with our earlier estimate of 1000 km. The direction of this motion agrees well with the apparent path across the spacecraft.

A structure of this size, in this plasma environment, may fall within ion scales. It is important to distinguish, however, that while the global size of the MH may extend to large scales, the current layer may not. When determining the contributions of current, however, it is more important to estimate the size of the current layer than the MH in its entirety as that is where the majority of the physics governing the MH takes place. The observations from MMS1 and MMS2 indicate the current layer width is on the order of 100 km.

4. Evidence of Electron Currents

MMS3 and MMS4 encountered two current layers that served as the boundary of the MH. The first (entering) boundary shows more high-amplitude, high-frequency wave behavior. The second, or exiting, boundary shows slightly lower amplitude and lower frequency E field activity and extends over a slightly longer period of time. The exiting boundary on MMS4, in particular, shows a smaller magnetic field depression with electric fields aligned along its boundaries.

Figure 2 shows the magnetic and electric field measurements as well as derived $E \times B$ velocities of MMS3 and MMS4 in the rotated coordinate system of the MH. There is minimal electric field activity aligned with the magnetic field. There are very active, positively directed, electric fields along the perp direction in both entering and exiting boundaries. The electric fields in the flow direction show primarily negative amplitude activity on the entering boundary and positive amplitude activity on the exiting boundary.

With the lack of particle measurements during this event, the view of the plasma environment is unavoidably incomplete. We can, however, rely on extensive research regarding the environment the spacecraft are in.

Table 1. Comparison of Derived and Observed Changes (Taken From the Mag Component From *E* and *B* Field Measurements in Magnetic Hole Coordinates) in Magnetic Field Strength With Their Associated Spacecraft and Boundary Layers

	MMS3		MMS4	
	ΔB_{mag} (nT)		ΔB_{mag} (nT)	
		Derived		Derived
Boundary Layer	Observed	$0.1 \leq n_e$ (cm^{-3}) ≤ 1.0	Observed	$0.1 \leq n_e$ (cm^{-3}) ≤ 1.0
Entering	−9.9	$-1.95 \leq \Delta B_{mag} \leq -19.5$	−8.5	$-2.3 \leq \Delta B_{mag} \leq -23$
Exiting	11	$1 \leq \Delta B_{mag} \leq 10$	7.3	$1.3 \leq \Delta B_{mag} \leq 13$

The ion Larmor radius in this region ranges from 100 to 1000 km [*Baumjohann et al.*, 1989; *Angelopoulos et al.*, 1992; *Cattell et al.*, 1992; *Ergun et al.*, 2015]. The sizes of the boundary layers are estimated to be on the order of 100 km, which is likely to be dominated by electron activity. This evidence indicates that this event may be classified as a small-scale MH.

The electric field measurements present a much more compelling argument. The E_{flow} signatures in Figure 2 are consistent with currents perpendicular to the magnetic field. This perpendicular current can induce an opposing magnetic field that causes an observed depletion in $|B|$. To determine whether this current could support the observed magnetic field depression, we derive the deviation of B_{mag} using measured values of $E \times B$ velocities perpendicular to the mag direction (V_{flow} and V_{perp}) in a derivation of Ampere's law, described in *Goodrich et al.* [2016].

The ΔB_{mag} derived from Ampere's law values are listed in comparison to the observed values in Table 1. The ΔB_{mag} was calculated over a range of 0.1 to 1 cm^{-3}, the typical range of observed particle densities in the BBF braking region [*Baumjohann et al.*, 1989]. The observed ΔB_{mag} of the entering boundary fall well within the range of the derived values with an optimal calculation where $n_e = 0.5$ cm^{-3} for both MMS3 and MMS4. The derived ΔB_{mag} values are consistently lower on the exiting boundary than the entering boundary. While it is clear that the $E \times B$ drifting electrons could support the entering boundary, it is not as clear that they could support the exiting boundary.

5. Evolution to Small Scales

The MH on MMS4 is particularly interesting as the entering and exiting boundaries show very different behavior. The entering boundary shows a decrease to the $|B|$ minimum in two different segments. The boundary first begins with a very sharp decrease in $|B|$, remains at the same value for ~0.5 s, then decreases to its minimum. The exiting boundary shows a steady $|B|$ increase for nearly the entirety of the exiting boundary. Before exiting the magnetic hole, the spacecraft sees a secondary magnetic hole embedded on the very edge of the exiting boundary, unseen by any other spacecraft.

A zoomed in view of the secondary MH is shown in Figure 3. The secondary MH shows an ~20% $|B|$ decrease (3 nT) below its initial value and has an estimated size of 96 km. The estimated boundary widths are 33 and 37 km for the entering and exiting boundaries, respectively. The MH shows E_{flow} signatures similar to that of its parent MH (negative on entering boundary and positive on exiting boundary), consistent with $E \times B$ drifting electrons on a smaller scale. The $|\Delta B_{mag}|$ values derived along the boundaries (outlined by the vertical lines in Figure 3) of this secondary MH range between 0.6 and 6 nT for both boundaries. At the optimum electron density (0.5 cm^{-3}) the derived $|\Delta B_{mag}|$ (~3 nT) matches the observed B_{mag} decrease.

The exiting boundary on MMS4 is observed over 1.4 s. There are higher amplitude *E* field signatures seen in the flow direction in the last 0.8 s within that boundary. More than half of that activity (0.48 s) is directly aligned with the secondary MH. The *E* field activity also dramatically decreases directly following the secondary magnetic hole. While it is clear that there are electron currents present in the exiting boundary of the MH seen on MMS4, the majority of the *E* field indicative of those currents are associated with the secondary MH, implying that the MH evolves to smaller spatial scales.

MMS is in the unique position of observing both previously mentioned types of small-scale MHs during the same event. Both types of MHs show electric fields consistent with $E \times B$ drifting electrons. These measurements imply that both depressions are supported by the same mechanism. The proximity of the two MHs and the similar processes strongly imply that they are linked. This event supports the possibility that small-scale

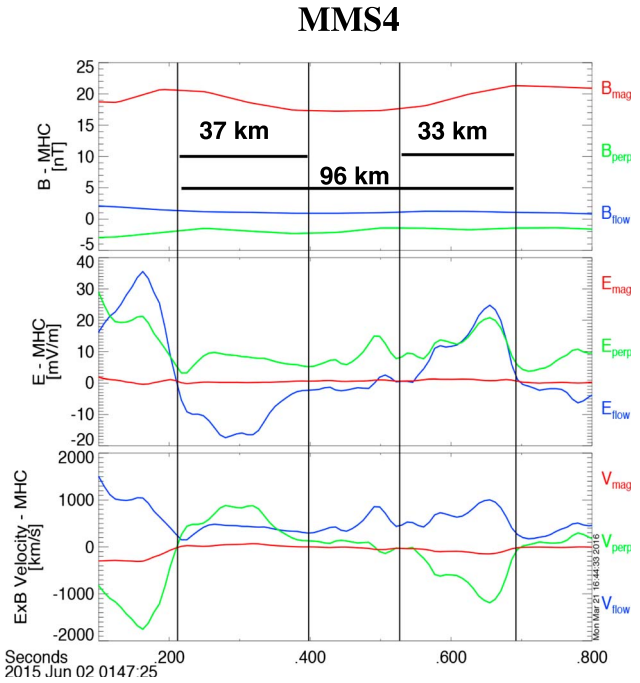

Figure 3. A closer look at the secondary magnetic hole embedded inside the exiting boundary of the larger magnetic hole seen on MMS4. This smaller magnetic hole decreases 3 nT (~20% drop) below its initial value. The electric fields measurements associated with this MH bear strong similarities to the MH that surrounds it (bipolar electric fields associated with its boundaries along the flow direction).

MHs are formed through strong electron currents that cascade to smaller spatial scales, resulting in smaller observed depressions in $|B|$.

6. Conclusions

We show evidence that the MMS spacecraft, particularly MMS4, observed electron currents perpendicular to the magnetic field that induces an opposing field that causes observed $|B|$ depressions. The spacecraft also show that those perpendicular electron currents cascade to smaller scales, resulting in smaller observed magnetic depressions (both spatially and in observed $|B|$). Additional MMS observations of very small-scale magnetic holes in the BBF braking region were reported by *Gershman et al.* [2016]. Those observations confirmed the presence of strong perpendicular electron currents in such events.

It is unclear how these currents are initially formed. It is possible that they are created through turbulent and bursty particle flows that are common in the BBF braking region. It is also possible they evolve from magnetic mirror-mode waves or another ion-scale instability. These observations do, however, offer insight into the dissipation processes that can occur within the BBF braking region. During phase 1X, which occurs on March–October 2016, MMS will once again encounter the BBF braking region in nearly full science mode. We hope to expand our understanding of these processes during phase 1X of the MMS mission.

Acknowledgments
This work was financially supported by the NASA MMS mission. Data from the MMS mission are publicly available at the MMS Science Data Center located at the Laboratory of Space Physics and can be obtained via https://lasp.colorado.edu/mms/sdc/public/. K.G. offers her immeasurable gratitude to the MMS team for their support and expertise.

References

Angelopoulos, V., W. Baumjohann, C. F. Kennel, F. V. Coronti, M. G. Kivelson, R. Pellat, R. J. Walker, H. Luehr, and G. Paschmann (1992), Bursty bulk flows in the inner central plasma sheet, *J. Geophys. Res.*, *97*, 4027–4039, doi:10.1029/91JA02701.

Angelopoulos, V., T. Mukai, and S. Kokubun (1999), Evidence for intermittency in Earth's plasma sheet and implications for self-organized criticality, *Phys. Plasmas*, *6*, 4161–4168, doi:10.1063/1.873681.

Balikhin, M. A., D. G. Sibeck, A. Runov, and S. N. Walker (2012), Magnetic holes in the vicinity of dipolarization fronts: Mirror or tearing structures?, *J. Geophys. Res.*, *117*, A08229, doi:10.1029/2012JA017552.

Baumjohann, W., G. Paschmann, and C. A. Cattell (1989), Average plasma properties in the central plasma sheet, *J. Geophys. Res.*, *94*, 6597–6606, doi:10.1029/JA094iA06p06597.

Borovsky, J. E., R. C. Elphic, H. O. Funsten, and M. F. Thomsen (1997), The Earth's plasma sheet as a laboratory for flow turbulence in high-[beta] MHD, *J. Plasma Phys.*, *57*, 1–34, doi:10.1017/S0022377896005259.

Burch, J. L., T. E. Moore, R. B. Torbert, and B. L. Giles (2016), Magnetospheric multiscale overview and science objectives, *Space Sci. Rev.*, *199*, 5–21, doi:10.1007/s11214-015-0164-9.

Burlaga, L. F., N. F. Ness, and M. H. Acuna (2007), Linear magnetic holes in a unipolar region of the heliosheath observed by Voyager 1, *J. Geophys. Res.*, *112*, A07106, doi:10.1029/2007JA012292.

Cattell, C. A., and F. S. Mozer (1982), Electric fields measured by ISEE-1 within and near the neutral sheet during quiet and active times, *Geophys. Res. Lett.*, *9*, 1041–1044, doi:10.1029/GL009i009p01041.

Cattell, C. A., C. W. Carlson, W. Baumjohann, and H. Luehr (1992), The MHD structure of the plasmasheet boundary. I—Tangential momentum balance and consistency with slow mode shocks, *Geophys. Res. Lett.*, *19*, 2083–2086, doi:10.1029/92GL02181.

Ergun, R. E., K. A. Goodrich, J. E. Stawarz, L. Andersson, and V. Angelopoulos (2015), Large-amplitude electric fields associated with bursty bulk flow braking in the Earth's plasma sheet, *J. Geophys. Res. Space Physics*, *120*, 1832–1844, doi:10.1002/2014JA020165.

Ergun, R. E., et al. (2016), The axial double probe and fields signal processing for the MMS mission, *Space Sci. Rev.*, *199*, 167–188, doi:10.1007/s11214-014-0115-x.

Fu, H. S., et al. (2013), Dipolarization fronts as a consequence of transient reconnection: In situ evidence, *Geophys. Res. Lett.*, *40*, 6023–6027, doi:10.1002/2013GL058620.

Ge, Y. S., J. P. McFadden, J. Raeder, V. Angelopoulos, D. Larson, and O. D. Constantinescu (2011), Case studies of mirror-mode structures observed by THEMIS in the near-Earth tail during substorms, *J. Geophys. Res.*, *116*, A01209, doi:10.1029/2010JA015546.

Gershman, D., et al. (2016), Electron dynamics in a subproton-gyroscale magnetic hole, *Geophys. Res. Lett.*, *43*, 4112–4118, doi:10.1002/2016GL068545.

Goodrich, K. A., R. E. Ergun, and J. E. Stawarz (2016), Electric fields associated with small-scale magnetic holes in the plasma sheet: Evidence for electron currents, *Geophys. Res. Lett.*, *43*, doi:10.1002/2016GL069601.

Haynes, C. T., D. Burgess, E. Camporeale, and T. Sundberg (2015), Electron vortex magnetic holes: A nonlinear coherent plasma structure, *Phys. Plasmas*, *22*(1), 012309, doi:10.1063/1.4906356.

Ji, X.-F., X.-G. Wang, W.-J. Sun, C.-J. Xiao, Q.-Q. Shi, J. Liu, and Z.-Y. Pu (2014), EMHD theory and observations of electron solitary waves in magnetotail plasmas, *J. Geophys. Res. Space Physics*, *119*, 4281–4289, doi:10.1002/2014JA019924.

Johnson, J. R., and C. Z. Cheng (1997), Global structure of mirror modes in the magnetosheath, *J. Geophys. Res.*, *102*, 7179–7190, doi:10.1029/96JA03949.

Lindqvist, P.-A., et al. (2016), The spin-plane double probe electric field instrument for MMS, *Space Sci. Rev.*, *199*, 137–165, doi:10.1007/s11214-014-0116-9.

Ohtani, S.-I., M. A. Shay, and T. Mukai (2004), Temporal structure of the fast convective flow in the plasma sheet: Comparison between observations and two-fluid simulations, *J. Geophys. Res.*, *109*, A03210, doi:10.1029/2003JA010002.

Pollock, C., et al. (2016), Fast plasma investigation for magnetospheric multiscale, *Space Sci. Rev.*, *199*, 331–406, doi:10.1007/s11214-016-0245-4.

Runov, A., V. Angelopoulos, M. I. Sitnov, V. A. Sergeev, J. Bonnell, J. P. McFadden, D. Larson, K.-H. Glassmeier, and U. Auster (2009), THEMIS observations of an earthward-propagating dipolarization front, *Geophys. Res. Lett.*, *36*, L14106, doi:10.1029/2009GL038980.

Runov, A., et al. (2011), Dipolarization fronts in the magnetotail plasma sheet, *Planet. Space Sci.*, *59*, 517–525, doi:10.1016/j.pss.2010.06.006.

Russell, C. T., L. K. Jian, J. G. Luhmann, T. L. Zhang, F. M. Neubauer, R. M. Skoug, X. Blanco-Cano, N. Omidi, and M. M. Cowee (2008), Mirror mode waves: Messengers from the coronal heating region, *Geophys. Res. Lett.*, *35*, L15101, doi:10.1029/2008GL034096.

Russell, C. T., et al. (2014), The magnetospheric multiscale magnetometers, *Space Sci. Rev.*, *199*, 189–256, doi:10.1007/s11214-014-0057-3.

Sitnov, M. I., M. Swisdak, and A. V. Divin (2009), Dipolarization fronts as a signature of transient reconnection in the magnetotail, *J. Geophys. Res.*, *114*, A04202, doi:10.1029/2008JA013980.

Soucek, J., E. Lucek, and I. Dandouras (2008), Properties of magnetosheath mirror modes observed by Cluster and their response to changes in plasma parameters, *J. Geophys. Res.*, *113*, A04203, doi:10.1029/2007JA012649.

Southwood, D. J., and M. G. Kivelson (1993), Mirror instability. I—Physical mechanism of linear instability, *J. Geophys. Res.*, *98*, 9181–9187, doi:10.1029/92JA02837.

Stawarz, J. E., R. E. Ergun, and K. A. Goodrich (2015), Generation of high-frequency electric field activity by turbulence in the Earth's magnetotail, *J. Geophys. Res. Space Physics*, *120*, 1845–1866, doi:10.1002/2014JA020166.

Sun, W. J., et al. (2012), Cluster and TC-1 observation of magnetic holes in the plasma sheet, *Ann. Geophys.*, *30*, 583–595, doi:10.5194/angeo-30-583-2012.

Sundberg, T., D. Burgess, and C. T. Haynes (2015), Properties and origin of subproton-scale magnetic holes in the terrestrial plasma sheet, *J. Geophys. Res. Space Physics*, *120*, 2600–2615, doi:10.1002/2014JA020856.

Tenerani, A., F. Califano, F. Pegoraro, and O. Le Contel (2012), Coupling between whistler waves and slow-mode solitary waves, *Phys. Plasmas*, *19*(5), 052103, doi:10.1063/1.4717764.

Tenerani, A., O. L. Contel, F. Califano, P. Robert, D. Fontaine, N. Cornilleau-Wehrlin, and J.-A. Sauvaud (2013), Cluster observations of whistler waves correlated with ion-scale magnetic structures during the 17 August 2003 substorm event, *J. Geophys. Res. Space Physics*, *118*, 6072–6089, doi:10.1002/jgra.50562.

Torbert, R. B., et al. (2016), The FIELDS instrument suite on MMS: Scientific objectives, measurements, and data products, *Space Sci. Rev.*, *199*, 105–135, doi:10.1007/s11214-014-0109-8.

Vörös, Z., W. Baumjohann, R. Nakamura, M. Volwerk, and A. Runov (2006), Bursty bulk flow driven turbulence in the Earth's plasma sheet, *Space Sci. Rev.*, *122*, 301–311, doi:10.1007/s11214-006-6987-7.

Weygand, J. M., et al. (2005), Plasma sheet turbulence observed by Cluster II, *J. Geophys. Res.*, *110*, A01205, doi:10.1029/2004JA010581.

Winterhalter, D., M. Neugebauer, B. E. Goldstein, E. J. Smith, B. T. Tsurutani, S. J. Bame, and A. Balogh (1995), Magnetic holes in the solar wind and their relation to mirror mode structures, *Space Sci. Rev.*, *72*, 201–204, doi:10.1007/BF00768780.